

# Geometry and superfluidity of the flat band in a non-Hermitian optical lattice

Peng He,<sup>1</sup> Hai-Tao Ding,<sup>1</sup> and Shi-Liang Zhu<sup>2,3,\*</sup>

<sup>1</sup>*National Laboratory of Solid State Microstructures and School of Physics, Nanjing University, Nanjing 210093, China*

<sup>2</sup>*Guangdong Provincial Key Laboratory of Quantum Engineering and Quantum Materials,  
School of Physics and Telecommunication Engineering,  
South China Normal University, Guangzhou 510006, China*

<sup>3</sup>*Guangdong-Hong Kong Joint Laboratory of Quantum Matter,  
Frontier Research Institute for Physics, South China Normal University, Guangzhou 510006, China*

(Dated: December 23, 2024)

We propose an ultracold-atom setting where a fermionic superfluidity with attractive s-wave interaction is uploaded in a non-Hermitian Lieb optical lattice. The existence of a real-energy flat band solution is revealed. We show that the interplay between the skin effect and flat-band localization leads to exotic localization properties. We develop a multiband mean-field description of this system and use both order parameters and superfluid weight to describe the phase transition. A relation between the superfluid weight and non-Hermitian quantum metric of the quantum states manifold is built. We find non-monotone criticality depending on the non-Hermiticity, and the skin effect prominently enhances the phase coherence of the pairing field, suggesting ubiquitous critical behavior of the non-Hermitian fermionic superfluidity.

## I. INTRODUCTION

A flat band is a dispersionless Bloch band with constant energy and heavy degeneracy for all quasi-momentum. The flat band arises as a result of destructive interference in bipartite quantum systems imposed by certain symmetries [1]. Systems with flat bands host intriguing features which are entirely governed by the quantum geometry and topology of the bands [2–8], facilitating the correlation in superconductivity [9–11], fractional quantum Hall states [12, 13], and frustration in ferromagnetism [14, 15]. For instance, the flat band yields a maximal critical temperature within the mean-field theory of superconductivity [16, 17], and plays an important role in the cuprates [18] and twisted-bilayer graphene [19–21]. The flat bands have been recognized and experimentally observed in the various contexts of condensed matter and synthetic quantum matter. Specifically, the Flat bands in Lieb lattice and Kagome lattice have been realized with the ultracold gases [22–25], photonic crystals [26–28], and electronic systems [30]. However, it is still an interesting direction to test flat-band physics in many varieties and classifications of states and phases meeting new progress of experiments.

In recent years, non-Hermitian states of matter have attracted considerable attention both theoretically and experimentally [31–33]. The systems described by non-Hermitian Hamiltonians are usually non-conserved, such as solids with finite quasi-particle lifetimes [34–37], artificial lattice [38] with gain and loss or nonreciprocity [39–44], and etc. Recent developments have revived interest in various physical aspects. The flat band has also been proposed in non-Hermitian systems [45–48], but still remains largely unexplored.

In this work, we study fermionic superfluidity with attractive s-wave interaction in an optical Lieb lattice. With the inclusion of both atom loss and inelastic collision, together with an auxiliary lattice, the system is effectively described by a non-Hermitian Hamiltonian with non-reciprocal hopping amplitudes and complex interaction strength. The Lieb lattice features a diabolic single Dirac cone intersected with a flat band [49, 50]. In the presence of non-hermiticity, the Dirac point will extend into a pair of exceptional points. As suggested by previous works, the non-Hermitian system with non-reciprocal hopping amplitudes will exhibit skin effect of which all bulk bands are pumped at the boundaries, as a manifestation of point gap topology associating with the exceptional points [51–56]. In this work, we demonstrate that the skin effect is forbidden by the geometric frustration of particle motion for the flat band. Furthermore, we find that the skin effect prominently enhances the phase stiffness of the fermionic superfluidity. We adopt mean-field description of the fermionic superfluidity by generalizing the non-Hermitian Bardeen-Cooper-Schrieffer (BCS) theory developed in Ref. [57] to the multiband case, leading to a non-Hermitian BdG Hamiltonian. In general, the emergence of the superconducting phase does not only require the form of the pairing field, but also the phase coherence of the pairs, which enables the Meissner effect [58]. We solve the gap equation and calculate the superfluid weight. We show that the superfluid weight for the non-Hermitian superfluidity is related with the integral of non-Hermitian metric tensor of the quantum state manifold over the Brillouin zone, which is a manifestation of nontrivial flat-band effect.

This paper is organized as follows. In Section II, we propose an ultracold-atom-based setup and present an effective non-Hermitian Hamiltonian. In section III, the band structures and the localization properties of the states are addressed in terms of interplay between the skin effect and destructive interference. Section IV devel-

\*Electronic address: [slzhu@nju.edu.cn](mailto:slzhu@nju.edu.cn)

ops a multiband mean-field description of the fermionic superfluid, and solve the gap equation. And in section V, we compute the superfluid weight and elucidate the unique criticality of the phase transition. Finally, a short conclusion is given in Sec. VI.

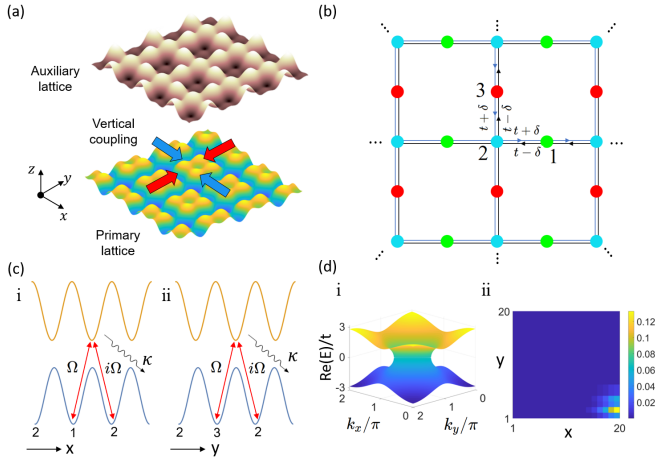


FIG. 1: (a) Schematic illustration of a proposed experimental setup with ultracold atoms in an optical lattice. (b) The Lieb lattice with non-reciprocal hopping, which has three inequivalent sites in one unit cell. (c) The cross-sections of (a) along (i) the x direction and (ii) the y direction, with sublattices 1,2 and 2,3 respectively.  $\kappa$  is the on-site decay rate in the auxiliary lattice. (d) The real part of the energy spectrum for  $\delta/t = 0.5$  and the corresponding bulk state distribution for the dispersive bands. Here we only show the two dispersive bands.

## II. MODEL HAMILTONIAN

We consider a gas of fermionic atoms in a two-dimensional optical lattice  $V_{\text{prm.}}$  with coherent coupling to the auxiliary degrees of freedom, as illustrated in Fig.

1. The primary lattice has a line-centered geometry, which could be experimentally realized by superimposing three pairs of laser beams with the following formation [22, 49, 50],

$$V_{\text{prm.}}(x, y) = -V_{\text{long}}^{(x)} \cos^2(k_L x) - V_{\text{long}}^{(y)} \cos^2(k_L y) - V_{\text{short}}^{(x)} \cos^2(2k_L x) - V_{\text{short}}^{(y)} \cos^2(2k_L y) - V_{\text{diag}}^{(x)} \cos^2(k_L(x - y)) - V_{\text{diag}}^{(y)} \cos^2(k_L(x + y)), \quad (1)$$

where  $k_L = 2\pi/\lambda$  is the wave number of the lattice and  $\lambda$  the wavelength of the lasers. The potential amplitudes  $V_{\text{long}}^{(x,y)}$ ,  $V_{\text{short}}^{(x,y)}$  and  $V_{\text{diag}}^{(x,y)}$  could be tuned by adjusting the laser intensities,  $\phi_{x,y}$  and  $\varphi$  are the phases of laser beams. For simplicity we choose  $(V_{\text{long}}^{(x)}, V_{\text{short}}^{(x)}, V_{\text{diag}}^{(x)}) = (V_{\text{long}}^{(y)}, V_{\text{short}}^{(y)}, V_{\text{diag}}^{(y)}) = (V_{\text{long}}, V_{\text{short}}, V_{\text{diag}})$ . To ensure the nearest-neighbor sites are coupled, the potential strength of the auxiliary lattice is tuned opposite to that of the primary lattice. The auxiliary lattice with decay is included to induce asymmetric hopping between the coupled sites, which generates the skin effect as we will see below.

Two equally populated magnetic sublevels of the hyperfine ground-state manifold are uploaded, to mimic the interacting spin-up and spin-down electrons moving in the lattice. Following the Ref. [29, 59, 61, 62], we propose to engineer a collective loss from a combination of on-site one-body losses of auxiliary lattice and two-body dissipations of the primary states. In experiment, the one-body loss could be generated by applying a radio frequency pulse to resonantly transfer the atoms to an irrelevant excited state, while the two-body dissipation could be induced by inelastic collisions with photoassociation process [63].

The full open-system dynamics in the rotating frame of reference can be written as

$$\dot{\rho}_t = -i[H_0 + \frac{\Omega}{2} \left( \sum_{i,j,\sigma} a_{i,j,2,\sigma}^\dagger (c_{i,j,1,\sigma} + i c_{i,j,2,\sigma}) + a_{i,j,1,\sigma}^\dagger (c_{i,j,1,\sigma} + i c_{i+1,j,2,\sigma}) + a_{i,j,3,\sigma}^\dagger (c_{i,j,2,\sigma} + i c_{i,j,3,\sigma}) + a_{i,j,2,\sigma}^\dagger (c_{i,j,2,\sigma} + i c_{i+1,j,3,\sigma}) + \text{H.c.} \right), \rho_t] + \sum_{i,j,\alpha} \mathcal{D}[a_{i,j,\alpha,\sigma}, c_{i,j,\alpha,\sigma}] \rho_t \quad (2)$$

where  $a_{i,j,\alpha,\sigma}$ 's ( $a_{i,j,\alpha,\sigma}^\dagger$ 's) denote the annihilation (creation) operators of the particles with spin  $\sigma = \uparrow, \downarrow$  in the auxiliary orbital centered at  $\mathbf{r}_{i,j,\alpha}$  ( $\alpha$  is the sublattice label),  $c_{i,j,\alpha,\sigma}$ 's ( $c_{i,j,\alpha,\sigma}^\dagger$ 's) denote corresponding annihilation (creation) operators of primary degrees of freedom,  $\Omega$  is the coupling strength between the primary lattice and auxiliary lattice,  $H_0$  is the Hamiltonian for the pri-

mary lattice, and  $\mathcal{D}[L]\rho \equiv L\rho L^\dagger - \frac{1}{2}\{L^\dagger L, \rho\}$  is the Lindblad superoperator.

In the regime that the on-site decay rate  $\kappa \gg \Omega$ , one can adiabatically eliminate the decay modes in the auxiliary lattice [59]. Thus the effective dynamics is well described by

$$\dot{\rho}_t = -i[H_0, \rho_t] + \mathcal{D}[L]\rho_t, \quad (3)$$

$$H_0 = - \sum_{\langle \mathbf{i}\alpha, \mathbf{j}\beta \rangle, \sigma} t_{\mathbf{i}\alpha, \mathbf{j}\beta}^\sigma c_{\mathbf{i}\alpha\sigma} c_{\mathbf{j}\beta\sigma}^\dagger - \tilde{U} \sum_{\mathbf{i}\alpha} n_{\mathbf{i}\alpha\uparrow} n_{\mathbf{i}\alpha\downarrow}, \quad (4)$$

$$L = \sum_{\langle \mathbf{i}\alpha, \mathbf{j}\beta \rangle, \sigma} \sqrt{2\gamma} (c_{\mathbf{i}\alpha\sigma} + i c_{\mathbf{j}\beta\sigma}) + \sum_{\mathbf{i}\alpha} \sqrt{\Gamma} c_{\mathbf{i}\alpha\downarrow} c_{\mathbf{i}\alpha\uparrow}, \quad (5)$$

where  $\gamma = \Omega^2/(2\kappa)$  and  $\Gamma$  is the two-body loss rate in the primary lattice, we only consider the tight-binding regime thus  $\langle \mathbf{i}\alpha, \mathbf{j}\beta \rangle$  runs over all nearest-neighbor sites [see Fig. 1 (b)], and we redefine  $\mathbf{i} = (i_x, i_y) = (i, j)$ .

If we only consider the dynamics over a short time, the quantum jump term  $\gamma L \rho_t L^\dagger$  is negligible. Thus we have an effective non-Hermitian Hamiltonian  $H_{\text{eff}} = H_0 - (i/2)L^\dagger L$  [57, 64]. With Fourier transformation  $c_{\mathbf{k}\alpha\sigma} = 1/\sqrt{N_c} \sum_{\mathbf{i}} e^{-i\mathbf{k}\cdot\mathbf{r}_{\mathbf{i}\alpha}} c_{\mathbf{i}\alpha\sigma}$ , the Hamiltonian in momentum space reads  $\mathcal{H}_{\text{eff}} = \mathcal{H}_{\text{kin}} + \mathcal{H}_{\text{int}} - \mu N$ . The kinetic term  $\mathcal{H}_{\text{kin}}$  is given by  $\mathcal{H}_{\text{kin}} = \sum_{\mathbf{k}} \Psi_{\mathbf{k}}^\dagger H_{\mathbf{k}} \Psi_{\mathbf{k}}$ , with  $\Psi_{\mathbf{k}} = [c_{\mathbf{k}\alpha\uparrow}, c_{\mathbf{k}\alpha\downarrow}]^T$ , and

$$H_{\mathbf{k}\uparrow} = H_{\mathbf{k}\downarrow} = a_{\mathbf{k}} \lambda_1 + b_{\mathbf{k}} \lambda_6, \quad (6)$$

where  $a_{\mathbf{k}} = 2t \cos(k_x/2) - 2i\delta \sin(k_x/2)$ ,  $b_{\mathbf{k}} = 2t \cos(k_y/2) + 2i\delta \sin(k_y/2)$  ( $\delta \equiv \gamma$ ), and  $\lambda_i$ 's are the  $i$ -th Gell-Mann matrices. The interaction term is given by  $\mathcal{H}_{\text{int}} = -U \sum_{\mathbf{k}\mathbf{k}',\alpha} c_{\mathbf{k}\alpha\uparrow}^\dagger c_{-\mathbf{k}\alpha\downarrow}^\dagger c_{-\mathbf{k}'\alpha\uparrow} c_{\mathbf{k}'\alpha\downarrow}$ , where interaction strength  $U \equiv \tilde{U} + i\Gamma/2$  becomes complex-valued due to the inelastic scattering. We note that our model can be regarded as a non-Hermitian extension of the Hubbard model on a Lieb lattice, which is firstly proposed in Ref. [4].

### III. FLAT BAND LOCALIZATION AND SKIN EFFECT

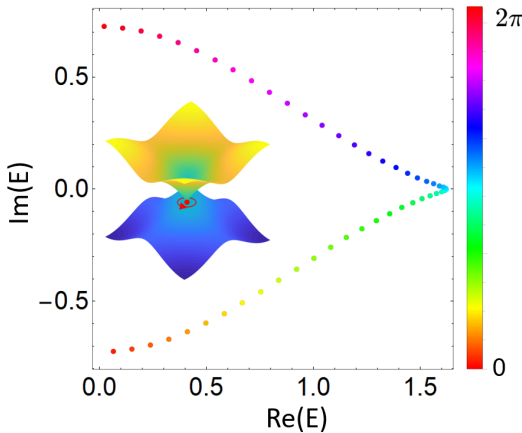


FIG. 2: The swapping of energy eigenvalues along the loop encircling the EP. The red line shows a path from  $\theta = 0$  to  $\theta = 2\pi$ .  $\theta \in [0, 2\pi]$  parametrizes the loop  $\mathcal{L}$ .

Let us start by considering the interaction-free Hamiltonian  $H_{\mathbf{k}}$ . The eigen-equation is given by  $H_{\mathbf{k}}|g_{n\mathbf{k}}\rangle = \varepsilon_{n\mathbf{k}}|g_{n\mathbf{k}}\rangle$  with the Bloch functions  $|g_{n\mathbf{k}}\rangle$  and the energy

dispersion  $\varepsilon_{n\mathbf{k}}$  ( $n = \pm, 0$ ). The upper and lower bands have complex-valued dispersion  $\varepsilon_{\pm} = \pm\sqrt{a_{\mathbf{k}}^2 + b_{\mathbf{k}}^2}$  [as illustrated in Fig. 1 (d,i)], while the middle band is purely real and strictly flat  $\varepsilon_0 = 0$ , as in the Hermitian limit. This is a result of the chiral symmetry of the Hamiltonian preserved under the non-Hermitian perturbation  $\hat{C}H_{\mathbf{k}}\hat{C} = -H_{\mathbf{k}}$ , with  $\hat{C} \equiv \text{diag}[1, -1, 1]$ . In contrast, for Lieb lattice considered in Ref. [45], which is in the presence of particle gain and loss on the sublattice sites, the non-Hermitian perturbation  $H_{NH} = -i\gamma\text{diag}[1, 0, -1]$  breaks the chiral symmetry. However, the flat band still could be restored from this system by virtue of artificial gauge potential and next-nearest-neighbor hopping.

The Lieb lattice features a single Dirac point at the corner of the Brillouin zone. In the presence of non-Hermiticity, the Hamiltonian  $H_{\mathbf{k}}$  has a pair of EPs at  $\mathbf{K}_{\pm} = \pm(\arccos(\frac{\delta^2-t^2}{\delta^2+t^2}), \arccos(\frac{\delta^2-t^2}{\delta^2+t^2}))$ , which are connected by a bulk Fermi arc, as shown in Fig. 1 (d,i).

As a bipartite quantum system from the chiral universality classes, the Lieb lattice admits destructive interference of states on flat band, which guarantees coherent cancellation of net particle flows thus leads to the localization of states [1, 65]. A single-particle state  $|\Phi\rangle = \sum_{\mathbf{r},\alpha} \mathcal{P}_{\mathbf{r},\alpha} c_{\mathbf{r},\alpha}^\dagger |0\rangle$  satisfies  $H_L|\Phi\rangle = 0$  if and only if

$$\sum_{\langle(\mathbf{r},\alpha),(\mathbf{r}',\beta)\rangle} \mathcal{P}_{\mathbf{r}',\beta} = 0, \quad \forall \mathbf{r}, \alpha, \quad (7)$$

where  $H_L$  is the lattice Hamiltonian in real space with  $U = 0$  and  $|0\rangle$  is the vacuum state. We call the state satisfying condition Eq.(7) a ring mode state. To see this, we consider straightforward manipulations on Wannier states,

$$H_L c_{11}^\dagger |0\rangle = [(t - \delta) c_{\mathbf{i}-\frac{a}{2}i_x, 2}^\dagger + (t + \delta) c_{\mathbf{i}+\frac{a}{2}i_x, 2}^\dagger] |0\rangle, \quad (8)$$

$$H_L c_{13}^\dagger |0\rangle = [(t + \delta) c_{\mathbf{i}-\frac{a}{2}i_y, 2}^\dagger + (t - \delta) c_{\mathbf{i}+\frac{a}{2}i_y, 1}^\dagger] |0\rangle, \quad (9)$$

thus we have a ring-mode state with  $\varepsilon = 0$ ,

$$|\Phi\rangle = \frac{1}{2} [t_1 c_{i,j,3}^\dagger - t_2 c_{i,j,1}^\dagger + t_1 c_{i+1,j+1,3}^\dagger - t_2 c_{i+1,j+1,1}^\dagger] |0\rangle, \quad (10)$$

where  $t_1 = \sqrt{\frac{t-\delta}{t+\delta}}$ ,  $t_2 = \sqrt{\frac{t+\delta}{t-\delta}}$ . Furthermore, any linear superposition of the single-plaquette ring-mode states given by Eq.(10) is also a solution, which gives rise to a large subspace with  $\varepsilon = 0$ . As revealed by Mielke [15], this can also be understood by the line graph theory. A line graph  $L(G)$  of a graph  $G$  is constructed with its vertex set the edge set of  $G(V, E)$ . The incidence matrix  $B(G) = (b_{ve})_{|V| \times |E|}$  (with unit entry  $b_{ve} = 1$  if the vertex  $v$  is incident to the edge  $e$  and zero otherwise) is related with the adjacency matrix  $A_L$  of the line graph by  $B^T B = 2I + A_L$ , due to the fact that every edge is always connected with two vertexes. If the number of vertexes  $n_V$  is smaller than that of the edges  $zn_V/2$ ,  $A_L$  will have a highly degenerate subspace with eigenvalue  $-2$ , such that  $B(G)$  has large zero space.

Due to the asymmetric hopping amplitudes, bulk states of non-Hermitian systems exhibit anomalous boundary localization, dubbed the skin effect. As shown in Fig. 1 (d,ii), all states with nonzero energy are pumped towards the direction with stronger hopping amplitude, which give rise to corner-state distributions. This is reminiscent of the second order skin effect studied in Ref. [60], but only happens for the two dispersive bands. The skin effect occurs as manifestation of the nontrivial point-gap topology signaling with the presence of the EPs, which is assigned with a winding number

$$\nu = \frac{1}{2\pi} \oint_{\mathcal{L}} \nabla_{\mathbf{q}} \arg[\varepsilon_+ - \varepsilon_-] \cdot d\mathbf{q}, \quad (11)$$

where  $\mathcal{L}$  is a closed loop encircling the EP. Each EP is associated with  $\nu = \pm \frac{1}{2}$ , as illustrated in Fig. 2. The bands with a point gap (finite interior in the complex spectra) have nonzero direct current  $J = \oint n(E, E^*) dE$  with  $n(E, E^*)$  the energy distribution, which gives rise to nonreciprocal pumping, *i.e.*, the skin effect [53]. In contrast, The flat band is purely real, and does not acquire a point gap in the complex plane, thus does not have the skin effect.

#### IV. MEAN-FIELD DESCRIPTION

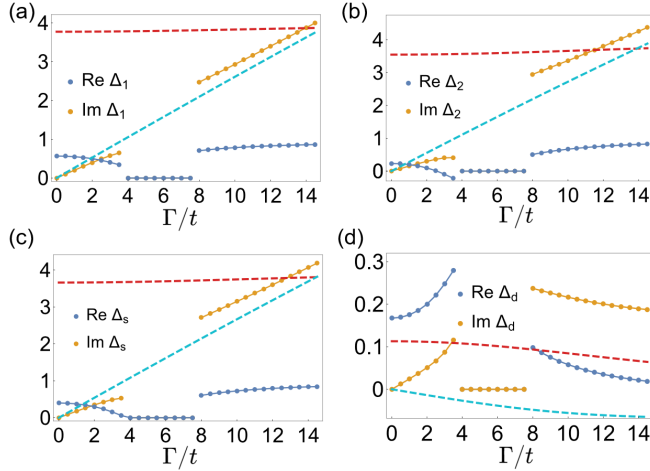


FIG. 3: Numerical solution of the order parameters as the function of  $\Gamma$  for  $\tilde{U} = 1.8$  at  $\beta = \infty$ . The red dashed line indicates the real part of the order parameters at strong interaction strength  $\tilde{U} = 10$ , while the blue dashed line indicates the imaginary part.

We adopt a mean-field description within the framework of BCS theory and decouple the interaction term as

$$\mathcal{H}_{\text{int}} \approx \sum_{\mathbf{k}, \alpha} \Delta_{\alpha} c_{\mathbf{k}\alpha\uparrow}^{\dagger} c_{-\mathbf{k}\alpha\downarrow}^{\dagger} + \bar{\Delta}_{\alpha} c_{-\mathbf{k}\alpha\uparrow} c_{\mathbf{k}\alpha\downarrow}, \quad (12)$$

where  $\Delta_{\alpha} = -U \sum_{\mathbf{k}} \langle \langle c_{-\mathbf{k}\alpha\downarrow} c_{\mathbf{k}\alpha\uparrow} \rangle \rangle$  and  $\bar{\Delta}_{\alpha} = -U \sum_{\mathbf{k}} \langle \langle c_{\mathbf{k}\alpha\uparrow}^{\dagger} c_{-\mathbf{k}\alpha\downarrow}^{\dagger} \rangle \rangle$ , and here we use the inner product

in the biorthonormal basis  $\langle \langle \mathcal{O} \rangle \rangle = \langle \tilde{\Psi} | \mathcal{O} | \Psi \rangle$ , with  $|\Psi\rangle$  ( $|\tilde{\Psi}\rangle$ ) the right (left) ground eigenstate of the Hamiltonian  $\mathcal{H}_{\text{eff}}$  and  $\mathcal{O}$  any operator. In Nambu representation  $\Psi_{\mathbf{k}} = [c_{\mathbf{k}\alpha\uparrow}, c_{-\mathbf{k}\alpha\downarrow}^{\dagger}]^T$ , The mean-filed Hamiltonian reads  $\mathcal{H}_{\text{MF}} = \sum_{\mathbf{k}} \Psi_{\mathbf{k}}^{\dagger} \mathcal{H}(\mathbf{k}) \Psi_{\mathbf{k}}$ , with the Bogoliubov-de Gennes (BdG) Hamiltonian

$$\mathcal{H}(\mathbf{k}) = \begin{bmatrix} H_{\mathbf{k}\uparrow} - \mu \mathbb{1} & \Delta \\ \Delta & -(H_{\mathbf{k}\downarrow} + \mu \mathbb{1}) \end{bmatrix}, \quad (13)$$

where  $\mathbb{1}$  is the  $3 \times 3$  identity matrix,  $\Delta = \text{diag}[\Delta_1, \Delta_2, \Delta_3]$ , and we have chosen the gauge for which  $\mathcal{H}_{\text{MF}}^{\dagger} = \mathcal{H}_{\text{MF}}$ , such that  $\Delta = \bar{\Delta}$ .

To obtain the superfluid weight, we consider the system subject to a uniform gauge field  $\mathbf{A}$ . By Peierls substitution  $\mathbf{k}$  to  $\mathbf{k} - \mathbf{q}$  ( $\mathbf{q} = e\mathbf{A}$ ) and diagonalizing the kinetic block, the Hamiltonian reads

$$\bar{\mathcal{H}}_{\mathbf{k}}(\mathbf{q}) = \begin{bmatrix} \varepsilon_{\mathbf{k}-\mathbf{q}} - \mu \mathbb{1} & \tilde{\mathcal{G}}_{\mathbf{k}-\mathbf{q}} \Delta \mathcal{G}_{\mathbf{k}+\mathbf{q}} \\ \tilde{\mathcal{G}}_{\mathbf{k}+\mathbf{q}} \Delta \mathcal{G}_{\mathbf{k}-\mathbf{q}} & -(\varepsilon_{\mathbf{k}+\mathbf{q}} - \mu \mathbb{1}) \end{bmatrix}, \quad (14)$$

where  $\varepsilon_{\mathbf{k}} = \text{diag}[\varepsilon_{n\mathbf{k}}]$ , and

$$\begin{aligned} \mathcal{G}_{\mathbf{k}} &= [ |g_{+\mathbf{k}}\rangle, |g_{0\mathbf{k}}\rangle, |g_{-\mathbf{k}}\rangle ], \\ \tilde{\mathcal{G}}_{\mathbf{k}} &= [\langle \tilde{g}_{+\mathbf{k}} |, \langle \tilde{g}_{0\mathbf{k}} |, \langle \tilde{g}_{-\mathbf{k}} | ]^T. \end{aligned} \quad (15)$$

The Hamiltonian (14) can be diagonalized as  $\bar{\mathcal{H}}_{\mathbf{k}} = \sum_{\mathbf{k}} E_{\mathbf{k}} (\tilde{\gamma}_{\mathbf{k}\uparrow} \gamma_{\mathbf{k}\uparrow} + \tilde{\gamma}_{-\mathbf{k}\downarrow} \gamma_{-\mathbf{k}\downarrow}) - \sum_{\mathbf{k}} E_{\mathbf{k}}$ , where  $\gamma_{\mathbf{k}\sigma} = [\gamma_{\mathbf{k}\alpha\sigma}]^T$ ,  $E_{\mathbf{k}} = \text{diag}[E_{+\mathbf{k}}, E_{0\mathbf{k}}, E_{-\mathbf{k}}]$ ,  $E_{\pm\mathbf{k}} = \sqrt{\varepsilon_{\mathbf{k}} + \Delta_s^2} \pm \Delta_d$ ,  $E_{0\mathbf{k}} = \Delta_1$ , with  $\Delta_d \equiv (\Delta_1 - \Delta_2)/2$  and  $\Delta_s \equiv (\Delta_1 + \Delta_2)/2$ . The quasiparticle operators are given by

$$\begin{aligned} \tilde{\gamma}_{\mathbf{k}\uparrow} &= u_{\mathbf{k}} c_{\mathbf{k}\uparrow}^{\dagger} - v_{\mathbf{k}} c_{-\mathbf{k}\downarrow}, \\ \tilde{\gamma}_{-\mathbf{k}\downarrow} &= v_{\mathbf{k}} c_{\mathbf{k}\uparrow} + u_{\mathbf{k}} c_{-\mathbf{k}\downarrow}^{\dagger}, \\ \gamma_{\mathbf{k}\uparrow} &= u_{\mathbf{k}} c_{\mathbf{k}\uparrow} - v_{\mathbf{k}} c_{-\mathbf{k}\downarrow}^{\dagger}, \\ \gamma_{\mathbf{k}\downarrow} &= v_{\mathbf{k}} c_{\mathbf{k}\uparrow}^{\dagger} + u_{\mathbf{k}} c_{-\mathbf{k}\downarrow}, \end{aligned} \quad (16)$$

where the coefficients  $u_{\mathbf{k}}$  and  $v_{\mathbf{k}}$  take values of

$$\begin{aligned} u_{\mathbf{k}} &= \frac{1}{\sqrt{2}} \begin{bmatrix} \cos \frac{\phi_{\mathbf{k}}}{2} & 0 & -\cos \frac{\phi_{\mathbf{k}}}{2} \\ 0 & 1 & 0 \\ \sin \frac{\phi_{\mathbf{k}}}{2} & 0 & \sin \frac{\phi_{\mathbf{k}}}{2} \end{bmatrix}, \\ v_{\mathbf{k}} &= \frac{1}{\sqrt{2}} \begin{bmatrix} \sin \frac{\phi_{\mathbf{k}}}{2} & 0 & -\sin \frac{\phi_{\mathbf{k}}}{2} \\ 0 & 1 & 0 \\ \cos \frac{\phi_{\mathbf{k}}}{2} & 0 & \cos \frac{\phi_{\mathbf{k}}}{2} \end{bmatrix}, \end{aligned} \quad (17)$$

with  $\cos \frac{\phi_{\mathbf{k}}}{2} = \frac{1}{\sqrt{2}} \sqrt{1 + \frac{\varepsilon_{\mathbf{k}}}{\sqrt{\varepsilon_{\mathbf{k}}^2 + \Delta_s^2}}}$ , and  $\sin \frac{\phi_{\mathbf{k}}}{2} = \frac{1}{\sqrt{2}} \sqrt{1 - \frac{\varepsilon_{\mathbf{k}}}{\sqrt{\varepsilon_{\mathbf{k}}^2 + \Delta_s^2}}}$ . From Eq. (16)-(17), the gap equation is obtained,

$$\Delta_1 = \frac{U}{4N_c} \sum_{\mathbf{k}} [t_{+, \mathbf{k}} \sin \phi_{\mathbf{k}} + t_{-, \mathbf{k}}] + \frac{U}{4} \tanh \frac{\beta \Delta_1}{2},$$

$$\Delta_2 = \frac{U}{2N_c} \sum_{\mathbf{k}} [t_{+, \mathbf{k}} \sin \phi_{\mathbf{k}} - t_{-, \mathbf{k}}],$$

$$\text{where } t_{\pm, \mathbf{k}} = \frac{1}{2} (\tanh \frac{\beta E_{+, \mathbf{k}}}{2} \pm \tanh \frac{\beta E_{-, \mathbf{k}}}{2}), \quad (18)$$

and  $N_c$  is the number of unit cells and we also have  $\Delta_1 = \Delta_3$  as a result of the sublattice (chiral) symmetry of the Hamiltonian. Note that the flat-band contribution only enters in the gap equations for the order parameter  $\Delta_1(\Delta_3)$ , due to the destructive interference on sublattice-2 [4].

We numerically solve the gap Eq. (18). The results are shown in Fig. 3. Here we only focus on the zero temperature solutions since the Fermi distribution does not give occupation probabilities due to the complex eigenenergies thus the temperature is not well defined for the non-Hermitian systems. Fig. 3 (a) and (b) show the pairing orders as functions of two-body loss  $\Gamma$ . Both  $\text{Re}\Delta_1$  and  $\text{Re}\Delta_2$  are suppressed by the two-body loss, and vanish after crossing a critical point. However, when the two-body loss is large enough,  $\text{Re}\Delta_1$  and  $\text{Re}\Delta_2$  acquire non-trivial values again and are even enhanced as the loss increases, which can be attributed to the localization-enhanced pairing due to the quantum Zeno effect for strong dissipation. This is reminiscent of the behavior of the pairing field in a single-band BCS system [57].

Although the pair field is suppressed by the loss, the gap  $\Delta_d$  in the mean-field spectrum is instead enhanced, due to slower decrement occurring in the pair field  $\text{Re}\Delta_1$

for sublattice-1 than for  $\text{Re}\Delta_2$ , as shown in Fig. 3 (d). This implies that the superfluidity is more robust against the two-body loss perturbation for the flat bands.

## V. SUPERFLUID WEIGHT

To compute the superfluid weight, we expand the free energy  $\mathfrak{F}(\mathbf{A})$  to second order  $\mathfrak{F}(\mathbf{A}) \approx \mathfrak{F}_0 + \frac{1}{2}V[D_s]_{ij}A_iA_j$ , where  $V$  is the system area,  $D_s$  is the superfluid weight, and  $\mathfrak{F}(\mathbf{A}) = -\frac{1}{\beta} \ln[e^{-\beta H_{\mathbf{k}}}]$ . Thus the superfluid weight is given by

$$[D_s]_{i,j} = \frac{1}{V\hbar^2} \frac{\partial^2 \mathfrak{F}}{\partial q_i \partial q_j} \Big|_{\mu, \mathbf{q}=0}, \quad (19)$$

where  $i, j = x, y$  are spatial indices.

For multiband superconducting phase, geometrical contribution enters the superfluid weight in the form of Fubini-Study metric integral of the quantum state manifold, beyond the conventional Landau-Ginzburg formalism. Specifically, For Hamiltonian Eq. (14), the superfluid weight reads

$$\begin{aligned} D_s^{i,j} = & \frac{1}{A\hbar^2} \sum_{\mathbf{k}} \left[ -2t_{+,\mathbf{k}} \cos \phi_{\mathbf{k}} \partial_{k_i} \partial_{k_j} \epsilon_{\mathbf{k}} - \frac{4t_{-,\mathbf{k}}}{E_{+,\mathbf{k}} - E_{-,\mathbf{k}}} \partial_{k_i} \epsilon_{\mathbf{k}} \partial_{k_j} \epsilon_{\mathbf{k}} \right. \\ & + 2\Delta_1 \left( \tanh \frac{\beta\Delta_1}{2} + t_{+,\mathbf{k}} \sin \phi_{\mathbf{k}} + t_{-,\mathbf{k}} \right) (\langle \partial_{k_i} \tilde{s}_{\mathbf{k}} | \partial_{k_j} s_{\mathbf{k}} \rangle + \langle \partial_{k_j} \tilde{s}_{\mathbf{k}} | \partial_{k_i} s_{\mathbf{k}} \rangle) \\ & \left. - \Delta_1^2 \langle \partial_{k_i} \tilde{s}_{\mathbf{k}} | s_{\mathbf{k}} \rangle \langle \tilde{s}_{\mathbf{k}} | \partial_{k_j} s_{\mathbf{k}} \rangle f(\mathbf{k}) - \Delta_1^2 (\langle \partial_{k_i} \tilde{s}_{\mathbf{k}} | c_{\mathbf{k}} \rangle \langle \tilde{c}_{\mathbf{k}} | \partial_{k_j} s_{\mathbf{k}} \rangle + (i \leftrightarrow j)) g(\mathbf{k}) \right]. \end{aligned} \quad (20)$$

The flat band has contribution,

$$[D_s]_{i,j}|_{\text{f.b.}} = \frac{\Delta_1}{\pi\hbar^2} \tanh \frac{\beta\Delta}{2} \mathcal{B}_{ij}|_{\text{f.b.}}, \quad (21)$$

where  $\mathcal{B}_{ij} = (2\pi)^{-1} \int_{\text{B.Z.}} d^2\mathbf{k} \mathfrak{G}_{ij}$  is the Brillouin-zone integral of the tensor, with its real part the quantum metric. The quantum metric is defined as  $\mathcal{M}_{ij} = \text{Re } \mathfrak{G}_{ij}$ , where

$$\begin{aligned} \mathfrak{G}_{ij} = & \frac{1}{2} [\langle \partial_{k_i} \tilde{g}_{0\mathbf{k}} | \partial_{k_j} g_{0\mathbf{k}} \rangle + \langle \partial_{k_j} \tilde{g}_{0\mathbf{k}} | \partial_{k_i} g_{0\mathbf{k}} \rangle \\ & - \langle \partial_{k_i} \tilde{g}_{0\mathbf{k}} | g_{0\mathbf{k}} \rangle \langle \tilde{g}_{0\mathbf{k}} | \partial_{k_j} g_{0\mathbf{k}} \rangle - \langle \partial_{k_j} \tilde{g}_{0\mathbf{k}} | g_{0\mathbf{k}} \rangle \langle \tilde{g}_{0\mathbf{k}} | \partial_{k_i} g_{0\mathbf{k}} \rangle]. \end{aligned} \quad (22)$$

In Fig. 4, we plot the geometric contribution and the conventional contribution respectively. Here we only focus on the diagonal components of the superfluid weight tensor  $[D_s]_{xx} = [D_s]_{yy} \approx D_s$ , since the off-diagonal components  $[D_s]_{xy/yx}$  is small. In the absence of non-Hermiticity, the superfluid weight  $D_s$  is enhanced as  $\tilde{U}$  increases in the weak-coupling regime. But  $D_s$  decreases after peaking at  $\tilde{U} \sim 4t$  with  $\tilde{U}$  further increases.

The non-monotonicity of  $D_s$  can be understood from the viewpoint of pseudopotential theory and a crossover from unbound Cooper pairs to performed fermions (or Bose liquid). Here we give a rough estimation. The s-wave scattering length  $a_s$  is rebuilt from the relation  $\tilde{U} = 4\pi\hbar^2 a_s / M$  with  $M$  the mass of atoms. Taking  $\hbar = M_r = 1$ , and the Fermi momentum  $k_F \sim \pi$ , we have  $1/k_F a_s \sim -1$  for  $-\tilde{U} = -4$ . After reaching the unitarity regime ( $-1 < 1/k_F a_s < 1$ ), the system will experience a crossover from the unbound Cooper pairs to the bounded pairs (molecules of fermions) with small pair size. The pairing happens on site, disordering the phase coherence of the pair filed, thus leading to a decrease of  $D_s$ . In the strong coupling regime, the superfluid weight is more robust to the non-Hermitian perturbations, as shown in Fig. 4.

Notably, we find that the skin effect enhances the superfluid weight in the weak-coupling regime, as shown in Fig. 4 (b) for the non-reciprocal BdG Hamiltonian. As revealed in Sec. III, in the presence of non-reciprocity, compact localized states for all bands have large density due to the skin effect and the destructive interfer-

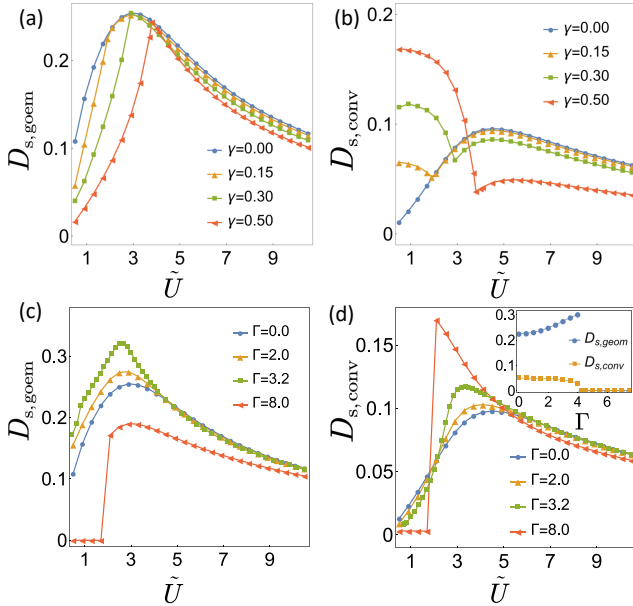


FIG. 4: (a) and (b) The geometric and conventional contribution in the superfluid weight at zero temperature with only non-reciprocity respectively. (c) and (d) The geometric and conventional contribution in the superfluid weight at zero temperature with only two-body loss. The inset in (d) shows the superfluid weights as functions of two-body loss strength  $\Gamma$  at  $\tilde{U} = 1.8$ .

ence, which enhances the overlapping of the Cooper pairs thus the coherence of the superconducting phase is promoted for the conventional part. In contrast, the geometric part decreases as non-reciprocity increases in the weak-coupling regime. On the other hand, for the Hamiltonian only with two-body loss, the superfluid weight is decreased by the loss as shown in Fig. 4 (d), since the two-body loss does not induce the skin effect.

Furthermore, we also find that the overall behavior of the geometric part mostly depends on the gap parameter  $\Delta_d$  after comparing the results in Fig. 4 and  $\Delta_d$  under same system parameters.

## VI. DISCUSSION AND CONCLUSION

In two dimension, the superfluid weight is related with the Berezinskii-Kosterlitz-Thouless transition. A larger superfluid weight at zero temperature usually implies a higher transition temperature [19]. Thus the superfluid weight can be estimated by the critical temperature in the experiment.

In conclusion, we have proposed a cold atomic setup with uniform s-wave interaction and atom loss, which is captured by a non-Hermitian Hamiltonian. We started by elucidating unique localization properties of the Bloch bands as an interplay of skin effect and the flat-band destructive interference. Then with the inclusion of complex s-wave interaction, we revealed novel critical-

ity of the non-Hermitian superfluidity related with the flat band within the framework of a mean-field BCS theory, in terms of both order parameters and the superfluid weight. We built a relation between the superfluid weight and the geometry of the Bloch states manifold in the non-Hermitian case. And we have also showed that the skin effect would optimize the superfluid weight. Our work provides an example that the skin effect can bring important physical implications.

## Acknowledgments

We thank Dan-Bo Zhang and Yu-Guo Liu for useful discussions. This work was supported by the Key-Area Research and Development Program of Guang-Dong Province (Grant No. 2019B030330001), the National Natural Science Foundation of China (Grants No. 12074180 and No. U1801661), the Key Project of Science and Technology of Guangzhou (Grants No. 201804020055 and No. 2019050001), and the National Key Research and Development Program of China (Grants No. 2016YFA0301800).

## Appendix A: Quantum metric tensor

In this section, we introduce the non-Hermitian quantum metric tensor, following the definition in Ref. [66]. For the set of the quantum states  $\{|g_{n\mathbf{k}}\rangle\}$  on the BZ torus, the density matrix is defined as,

$$\rho_n(\mathbf{k}) \equiv |\tilde{g}_{n\mathbf{k}}\rangle\langle g_{n\mathbf{k}}|. \quad (\text{A1})$$

The fidelity between  $\rho_n(\mathbf{k})$  and  $\rho_n(\mathbf{k} + \delta\mathbf{k})$  is given by

$$F(\rho_n(\mathbf{k}), \rho_n(\mathbf{k} + \delta\mathbf{k})) = \text{tr} \sqrt{|\rho_n^{1/2}(\mathbf{k})\rho_n(\mathbf{k} + \delta\mathbf{k})\rho_n^{1/2}(\mathbf{k})|}. \quad (\text{A2})$$

The Fubini-Study metric defines a distance of nearby states on the BZ torus,

$$ds^2 := 2[1 - F(\rho_n(\mathbf{k}), \rho_n(\mathbf{k} + \delta\mathbf{k}))]. \quad (\text{A3})$$

By expanding the states  $|g_{n\mathbf{k}+\delta\mathbf{k}}\rangle$  to second order, we have

$$ds^2 = \frac{1}{2} \text{Re}(\langle \partial_\mu \tilde{g}_{n\mathbf{k}} | \partial_\nu g_{n\mathbf{k}} \rangle + \langle \partial_\nu \tilde{g}_{n\mathbf{k}} | \langle \lambda | \partial_\mu g_{n\mathbf{k}} \rangle - 2\langle \partial_\mu \tilde{g}_{n\mathbf{k}} | g_{n\mathbf{k}} \rangle \langle \tilde{g}_{n\mathbf{k}} | \partial_\nu g_{n\mathbf{k}} \rangle) dk^\mu dk^\nu. \quad (\text{A4})$$

Here to shorten notations we define  $\partial_\mu \equiv \partial_{k_\mu}$ . After noting that  $\langle \partial_\mu \tilde{g}_{n\mathbf{k}} | g_{n\mathbf{k}} \rangle \langle \tilde{g}_{n\mathbf{k}} | \partial_\nu g_{n\mathbf{k}} \rangle = \langle \partial_\nu \tilde{g}_{n\mathbf{k}} | g_{n\mathbf{k}} \rangle \langle \tilde{g}_{n\mathbf{k}} | \partial_\mu g_{n\mathbf{k}} \rangle$ , we can rewrite the quantum metric tensor as

$$\mathcal{M}_{ij} = \frac{1}{2} \text{Re}[\langle \partial_{k_i} \tilde{g}_{n\mathbf{k}} | \partial_{k_j} g_{n\mathbf{k}} \rangle + \langle \partial_{k_j} \tilde{g}_{n\mathbf{k}} | \partial_{k_i} g_{n\mathbf{k}} \rangle - \langle \partial_{k_i} \tilde{g}_{n\mathbf{k}} | g_{n\mathbf{k}} \rangle \langle \tilde{g}_{n\mathbf{k}} | \partial_{k_j} g_{n\mathbf{k}} \rangle - \langle \partial_{k_j} \tilde{g}_{n\mathbf{k}} | g_{n\mathbf{k}} \rangle \langle \tilde{g}_{n\mathbf{k}} | \partial_{k_i} g_{n\mathbf{k}} \rangle]. \quad (\text{A5})$$

## Appendix B: Derivation details of the superfluid weight

By virtue of the biorthogonal representation, we derive the superfluid weight of the non-Hermitian superfluidity, following the method originally developed in the Refs. [3, 4, 67]. The first derivative of the free energy  $\Omega(\mathbf{q})$  is the current density,

$$\mathbf{J}(\mathbf{q}) = \frac{-1}{2V\hbar} \sum_{\mathbf{k}} \text{Tr} [\text{sign}(E_{\mathbf{k}}(\mathbf{q})) \mathcal{W}_{\mathbf{k}}^T(\mathbf{q}) \partial_{\mathbf{q}} H_{\mathbf{k}}(\mathbf{q}) \mathcal{W}_{\mathbf{k}}(\mathbf{q})], \quad (\text{B1})$$

$$-\partial_{\mathbf{q}} H_{\mathbf{k}}(\mathbf{q}) = \begin{bmatrix} \partial_{\mathbf{k}} \varepsilon_{\mathbf{k}-\mathbf{q}} & \partial_{\mathbf{q}} \mathcal{D}_{\mathbf{k}}(\mathbf{q}) \\ -\partial_{\mathbf{q}} \mathcal{D}_{\mathbf{k}}(-\mathbf{q}) & \partial_{\mathbf{k}} \varepsilon_{\mathbf{k}+\mathbf{q}} \end{bmatrix}, \quad (\text{B2})$$

Here we define  $\mathcal{D}_{\mathbf{k}} \equiv \tilde{\mathcal{G}}_{\mathbf{k}-\mathbf{q}} \Delta \mathcal{G}_{\mathbf{k}+\mathbf{q}}$ , and

$$\mathcal{W}_{\mathbf{k}} \equiv \begin{bmatrix} u_{\mathbf{k}} & -v_{\mathbf{k}} \\ v_{\mathbf{k}} & u_{\mathbf{k}} \end{bmatrix}. \quad (\text{B3})$$

Straightforward calculation shows that,

$$\tilde{\mathcal{G}}_{\mathbf{k}_1} \Delta \mathcal{G}_{\mathbf{k}_2} = \frac{\Delta_A}{2} \begin{bmatrix} \langle \tilde{s}_{\mathbf{k}_1} | s_{\mathbf{k}_2} \rangle & \sqrt{2} \langle \tilde{s}_{\mathbf{k}_1} | c_{\mathbf{k}_2} \rangle & \langle \tilde{s}_{\mathbf{k}_1} | s_{\mathbf{k}_2} \rangle \\ \sqrt{2} \langle \tilde{c}_{\mathbf{k}_1} | s_{\mathbf{k}_2} \rangle & 2 \langle \tilde{c}_{\mathbf{k}_1} | c_{\mathbf{k}_2} \rangle & \sqrt{2} \langle \tilde{c}_{\mathbf{k}_1} | s_{\mathbf{k}_2} \rangle \\ \langle \tilde{s}_{\mathbf{k}_1} | s_{\mathbf{k}_2} \rangle & \sqrt{2} \langle \tilde{s}_{\mathbf{k}_1} | c_{\mathbf{k}_2} \rangle & \langle \tilde{s}_{\mathbf{k}_1} | s_{\mathbf{k}_2} \rangle \end{bmatrix} + \frac{\Delta_B}{2} \begin{bmatrix} 1 & 0 & -1 \\ 0 & 0 & 0 \\ -1 & 0 & 1 \end{bmatrix}. \quad (\text{B4})$$

Here we denote  $\mathbf{k}_1 = \mathbf{k} - \mathbf{q}$  and  $\mathbf{k}_2 = \mathbf{k} + \mathbf{q}$ , and we introduce a two-component spinor  $|s_{\mathbf{k}}\rangle$  (together with  $\langle \tilde{s}_{\mathbf{k}} |$ ) and its partner  $|c_{\mathbf{k}}\rangle = i\sigma_y |s_{\mathbf{k}}\rangle$  (together with  $\langle \tilde{c}_{\mathbf{k}} |$ ),

$$|s_{\mathbf{k}}\rangle = \frac{1}{\sqrt{a_{\mathbf{k}}^2 + b_{\mathbf{k}}^2}} \begin{bmatrix} a_{\mathbf{k}} \\ b_{\mathbf{k}} \end{bmatrix}, \quad |c_{\mathbf{k}}\rangle = \frac{1}{\sqrt{a_{\mathbf{k}}^2 + b_{\mathbf{k}}^2}} \begin{bmatrix} b_{\mathbf{k}} \\ -a_{\mathbf{k}} \end{bmatrix}, \quad (\text{B5})$$

$$\langle \tilde{s}_{\mathbf{k}} | = [a_{\mathbf{k}}, b_{\mathbf{k}}] / \sqrt{a_{\mathbf{k}}^2 + b_{\mathbf{k}}^2}, \quad \langle \tilde{c}_{\mathbf{k}} | = [b_{\mathbf{k}}, -a_{\mathbf{k}}] / \sqrt{a_{\mathbf{k}}^2 + b_{\mathbf{k}}^2}. \quad (\text{B6})$$

Note that  $\langle \tilde{s}_{\mathbf{k}}(\tilde{c}_{\mathbf{k}}) |$  is not the Hermitian conjugate of  $|s_{\mathbf{k}}(c_{\mathbf{k}})\rangle$ . The derivative of the current density gives rise to the superfluid weight after setting  $\mathbf{q} = 0$ ,

$$[D_s]_{ij} = \frac{1}{V\hbar^2} \frac{\partial^2 \mathfrak{F}}{\partial q_i \partial q_j} \Big|_{\mathbf{q}=0} = [D_{s,\text{conv}}]_{i,j} + [D_{s,\text{geom}}]_{i,j}, \quad (\text{B7})$$

$$[D_{s,\text{conv}}]_{ij} = \frac{2}{V\hbar^2} \sum_{\mathbf{k}} \text{Tr} [(v_{\mathbf{k}} \frac{1}{e^{-\beta E_{\mathbf{k}}+1}} v_{\mathbf{k}}^T + u_{\mathbf{k}} \frac{1}{e^{\beta E_{\mathbf{k}}+1}} u_{\mathbf{k}}^T) \partial_{k_i} \partial_{k_j} \varepsilon_{\mathbf{k}}], \quad (\text{B8})$$

$$\begin{aligned} [D_{s,\text{geom}}]_{ij} = & \frac{1}{V\hbar^2} \{ 2 \sum_{\mathbf{k}} \text{Tr} [(u_{\mathbf{k}} v_{\mathbf{k}}^T - u_{\mathbf{k}} \frac{1}{e^{\beta E_{\mathbf{k}}+1}} v_{\mathbf{k}}^T - v_{\mathbf{k}} \frac{1}{e^{\beta E_{\mathbf{k}}+1}} v_{\mathbf{k}}^T) \partial_{q_i} \partial_{q_j} \mathcal{D}_{\mathbf{k}}(\mathbf{q}=0)] \\ & - \frac{1}{2} \sum_{\mathbf{k}} \sum_{a,b} [T_{\mathbf{k}}]_{a,b} [N_{\mathbf{k},i}]_{a,b} [N_{\mathbf{k},j}]_{b,a} \}, \end{aligned} \quad (\text{B9})$$

where  $N_{\mathbf{k},i} = \mathcal{W}_{\mathbf{k}}^T(\mathbf{q}=0) \partial_{q_i} \bar{H}_{\mathbf{k}}(\mathbf{q}=0) \mathcal{W}_{\mathbf{k}}(\mathbf{q}=0)$ , and the off-diagonal components of  $T_{\mathbf{k}}$   $[T_{\mathbf{k}}]_{a,b} = [\tanh(\beta E_{\mathbf{k}}/2)]_{a,a} - [\tanh(\beta E_{\mathbf{k}}/2)]_{b,b} / ([E_{\mathbf{k}}]_{a,a} -$

$[E_{\mathbf{k}}]_{b,b})$ , and the diagonal components  $[T_{\mathbf{k}}]_{a,a} = [\beta/2 \cosh^2(\beta E_{\mathbf{k}}/2)]_{a,a}$ .

[1] Z. Liu, F. Liu, and Y. S. Wu, Exotic electronic states in the world of flat bands: From theory to material, Chin.

Phys. B **23**, 077308 (2014).

[2] K. Sun, Z. Gu, H. Katsura, and S. Das Sarma, Nearly

Flatbands with Nontrivial Topology, *Phys. Rev. Lett.* **106**, 236803 (2011).

[3] S. Peotta and P. Törmä, Superfluidity in topologically nontrivial flat bands, *Nat. Commun.* **6**, 8944 (2015).

[4] A. Julku, S. Peotta, T.-I. Vanhala, D.-H. Kim, and P. Törmä, Geometric Origin of Superfluidity in the Lieb-Lattice Flat Band, *Phys. Rev. Lett.* **117**, 045303 (2016).

[5] P. Törmä, L. Liang, and S. Peotta, Quantum metric and effective mass of a two-body bound state in a flat band, *Phys. Rev. B* **98**, 220511(R) (2018).

[6] J. Rhim, K. Kim, and B. Yang, Quantum distance and anomalous Landau levels of flat bands, *Nature* **584**, 59 (2020).

[7] C. Danieli, A. Andreevov, and S. Flach, Many-body flat-band localization, *Phys. Rev. B* **102**, 041116(R) (2020).

[8] Y. Kuno, T. Orito, and I. Ichinose, Flat-band many-body localization and ergodicity breaking in the Creutz ladder, *New J. Phys.* **22** 013032 (2020).

[9] E. Tang, and L. Fu, Strain-induced partially flat band, helical snake states and interface superconductivity in topological crystalline insulators, *Nature Phys.* **10**, 964 (2014).

[10] R. Mondaini, G.-G. Batrouni, and B. Grémaud, Pairing and superconductivity in the flat band: Creutz lattice, *Phys. Rev. B* **98**, 155142 (2018).

[11] J. Mao, S.P. Milovanović, M. Andelković, et al., Evidence of flat bands and correlated states in buckled graphene superlattices, *Nature* **584**, 215 (2020).

[12] T. Neupert, L. Santos, C. Chamon, and C. Mudry, Fractional Quantum Hall States at Zero Magnetic Field, *Phys. Rev. Lett.* **106**, 236804 (2011).

[13] E. J. Breholtz and Z. Liu, Topological flat band models and fractional Chern insulators, *Int. J. Mod. Phys. B* **27**, 1330017 (2013).

[14] E. H. Lieb, Two Theorems on the Hubbard Model, *Phys. Rev. Lett.* **62**, 1201 (1989).

[15] A Mielke, Ferromagnetic ground states for the Hubbard model on line graphs, *J. Phys. A: Math. Gen.* **24**, L73 (1991).

[16] N. B. Kopnin, T. T. Heikkil?, and G. E. Volovik, Hightemperature surface superconductivity in topological flatband systems, *Phys. Rev. B* **83**, 220503(R) (2011).

[17] V. I. Iglovikov, F. Hébert, B. Grémaud, G. G. Batrouni, and R. T. Scalettar, Superconducting transitions in flat-band systems, *Phys. Rev. B* **90**, 094506 (2014).

[18] V. J. Emery, Theory of High- $T_c$  Superconductivity in Oxides, *Phys. Rev. Lett.* **58**, 2794 (1987).

[19] F. Xie, Z. Song, B. Lian, and B. A. Bernevig, Topology-Bounded Superfluid Weight in Twisted Bilayer Graphene, *Phys. Rev. Lett.* **124**, 167002 (2020)

[20] X. Hu , T. Hyart, D. I. Pikulin, and Enrico Rossi, Geometric and Conventional Contribution to the Superfluid Weight in Twisted Bilayer Graphene, *Phys. Rev. Lett.* **123**, 237002 (2019).

[21] A. Julku, T. J. Peltonen, L. Liang, et al., Superfluid weight and Berezinskii-Kosterlitz-Thouless transition temperature of twisted bilayer graphene, *Phys Rev. B* **101**, 060505(R) (2020).

[22] S. Taie, H. Ozawa, T. Ichinose, T. Nishio, S. Nakajima and Y. Takahashi, Coherent driving and freezing of bosonic matter wave in an optical Lieb lattice, *Sci. Adv.* **1**, 1500854 (2015).

[23] T.-H. Leung, M. N. Schwarz, S.-W. Chang, C. D. Brown1, G. Unnikrishnan , and D. Stamper-Kurn, Interaction-Enhanced Group Velocity of Bosons in the Flat Band of an Optical Kagome Lattice, *Phys. Rev. Lett.* **125**, 133001 (2020).

[24] G.-W. Chern, C.-C. Chien, and M. Di Ventra, Dynamically generated flat-band phases in optical kagome lattices, *Phys. Rev. A* **90**, 013609 (2014).

[25] G.-B. Jo, J. Guzman, and C. K. Thomas, Ultracold Atoms in a Tunable Optical Kagome Lattice, *Phys. Rev. Lett.* **108**, 045305 (2012).

[26] D. Guzmán-Silva, C. Mejía-Cortés, M. A. Bandres, M. C. Rechtsman, S. Weimann, S. Nolte, M. Segev, A. Szameit, and R. A. Vicencio, Experimental observation of bulk and edge transport in photonic Lieb lattices, *New J. Phys.* **16**, 063061 (2014).

[27] R. A. Vicencio, C. Cantillano, L. Morales-Inostroza, et al., Observation of Localized States in Lieb Photonic Lattices, *Phys. Rev. Lett.* **114**, 245503 (2015).

[28] S. Mukherjee, A. Spracklen, D. Choudhury, N. Goldman, P. Öhberg, E. Andersson, and R. R. Thomson, Observation of a Localized Flat-Band State in a Photonic Lieb Lattice, *Phys. Rev. Lett.* **114**, 245504 (2015).

[29] Z. Gong, Y. Ashida, K. Kawabata, K. Takasan, S. Higashikawa, and M. Ueda, Topological phases of non-Hermitian systems, *Phys. Rev. X* **8**, 031079 (2018).

[30] M. Slot, T. Gardenier, P. Jacobse, et al., Experimental realization and characterization of an electronic Lieb lattice, *Nature Phys* **13**, 672C676 (2017).

[31] A. Ghatak and T. Das, New topological invariants in non-Hermitian systems, *J. Phys. D: Appl. Phys.* **31**, 263001 (2019).

[32] E. J. Bergholtz, J. C. Budich, and F. K. Kunst, Exceptional Topology of Non-Hermitian Systems, *arXiv:1912.10048* (2019).

[33] Y. Ashida, Z. Gong, and M. Ueda, Non-Hermitian Physics, *arXiv:2006.01837* (2020).

[34] V. Kozii and L. Fu, Non-Hermitian topological theory of finite-lifetime quasiparticles: prediction of bulk Fermi arc due to exceptional point, *arXiv:1708.05841* (2017).

[35] H. Shen, B. Zhen, and L. Fu, Topological band theory for non-Hermitian Hamiltonians, *Phys. Rev. Lett.* **120**, 146402 (2018).

[36] M. Papaj, H. Isobe, and L. Fu, Nodal arc of disordered Dirac fermions and non-Hermitian band theory, *Phys. Rev. B* **99**, 201107 (2019).

[37] X. Shen, F. Wang, Z. Li, and Z. Wu, Landau-Zener-Stückelberg interferometry in PT-symmetric non-Hermitian models, *Phys. Rev. A* **100**, 062514 (2019).

[38] D. W. Zhang, Y. Q. Zhu, Y. X. Zhao, H. Yan, and S. L. Zhu, Topological quantum matter with cold atoms, *Adv. Phys.* **67**, 253 (2018).

[39] D.-W. Zhang, L.-Z. Tang, L.-J. Lang, H. Yan, and S.-L. Zhu, Non-Hermitian topological Anderson insulator, *Sci. China-Phys. Mech. Astron.* **63**, 267062 (2020).

[40] H. Jiang, L.-J. Lang, C. Yang, S.-L. Zhu, and S. Chen, Interplay of non-Hermitian skin effects and Anderson localization in nonreciprocal quasiperiodic lattices, *Phys. Rev. B* **100**, 054301 (2019).

[41] J. Li, A. K. Harter, J. Liu, L. Melo1, Y. N. Joglekar, and L. Luo, Observation of parity-time symmetry breaking transitions in a dissipative Floquet system of ultracold atoms, *Nat. Commun.* **10**, 855 (2019).

[42] H. Zhou et al., Observation of bulk Fermi arc and polarization half charge from paired exceptional points, *Sci.*

ence, **359**, 1009-1012 (2018).

[43] A. Cerjan et al., Experimental realization of a Weyl exceptional ring, *Nat. Photonics* **13**, 623-628 (2019).

[44] L. Z. Tang, L. F. Zhang, G. Q. Zhang, and D.-W. Zhang, Topological Anderson insulators in two-dimensional non-Hermitian disordered systems, *Phys. Rev. A* **101**, 063612 (2020).

[45] S. M. Zhang, and L. Jin., Flat band in two-dimensional non-Hermitian optical lattices, *Phys. Rev. A* **100**, 043808 (2019).

[46] L. Jin, Flat band induced by the interplay of synthetic magnetic flux and non-Hermiticity, *Phys. Rev. A* **99**, 033810 (2019).

[47] D. Leykam, S. Flach, and Y. D. Chong, Flat bands in lattices with non-Hermitian coupling, *Phys. Rev. B* **96**, 064305 (2017).

[48] H. Ramezani, Non-Hermiticity-induced flat band, *Phys. Rev. A* **96**, 011802(R) (2017).

[49] R. Shen, L. B. Shao, B. Wang, and D. Y. Xing, Single Dirac cone with a flat band touching on line-centered-square optical lattices, *Phys. Rev. B* **81**, 041410 (2010).

[50] C. Weeks and M. Franz, Topological insulators on the Lieb and perovskite lattices. *Phys. Rev. B* **82**, 085310 (2010).

[51] S. Yao and Z. Wang, Edge states and topological invariants of non-Hermitian systems, *Phys. Rev. Lett.* **121**, 086803 (2018).

[52] F. Song, S. Yao, and Z. Wang, Non-Hermitian skin effect and chiral damping in open quantum systems, *Phys. Rev. Lett.* **123**, 170401 (2019).

[53] K. Zhang, Z. Yang, and C. Fang, Correspondence between Winding Numbers and Skin Modes in Non-Hermitian Systems, *Phys. Rev. Lett.* **125**, 126402 (2020).

[54] L. Li, C. H. Lee, and J. Gong, Topological Switch for Non-Hermitian Skin Effect in Cold-Atom Systems with Loss, *Phys. Rev. Lett.* **124**, 250402 (2020).

[55] N. Okuma, K. Kawabata, K. Shiozaki, and M. Sato, Topological Origin of Non-Hermitian Skin Effects, *Phys. Rev. Lett.* **124**, 086801 (2020).

[56] L. Jin, Z. Song, Bulk-boundary correspondence in a non-Hermitian system in one dimension with chiral inversion symmetry, *Phys. Rev. B* **99**, 081103 (2019).

[57] K. Yamamoto, M. Nakagawa, K. Adachi, K. Takasan, M. Ueda, and N. Kawakami, Theory of non-hermitian fermionic superfluidity with a complex-valued interaction, *Phys. Rev. Lett.* **123**, 123601 (2019).

[58] J. Corson, R. Mallozzi, J. Orenstein, J. Eckstein, and I. Bozovic, Vanishing of phase coherence in underdoped  $\text{Bi}_2\text{Sr}_2\text{CaCu}_2\text{O}_{8+\delta}$ . *Nature* **398**, 221 (1999).

[59] T. Liu, Y. Zhang, Q. Ai, Z. Gong, K. Kawabata, M. Ueda, and F. Nori, Second-Order Topological Phases in Non-Hermitian Systems. *Phys. Rev. Lett.* **122**, 076801 (2019).

[60] C. H. Lee, L. Li, and J. Gong, Hybrid Higher-Order Skin Topological Modes in Nonreciprocal Systems, *Phys. Rev. Lett.* **123**, 016805 (2019).

[61] M. Müller, S. Diehl, G. Pupillo, and P. Zoller, Engineered Open Systems and Quantum Simulations with Atoms and Ions, *Adv. At. Mol. Opt. Phys.* **61**, 1 (2012).

[62] S. Diehl, E. Rico, M.A. Baranov, and P. Zoller, Topology by Dissipation in Atomic Quantum Wires, *Nat. Phys.* **7**, 971 (2011).

[63] T. Tomita, S. Nakajima, I. Danshita, Y. Takasu, and Y. Takahashi, Observation of the Mott insulator to superfluid crossover of a driven-dissipative Bose-Hubbard system, *Sci. Adv.* **3**, e1701513 (2017).

[64] J.F. Poyatos, J.I. Cirac, and P. Zoller, Quantum Reservoir Engineering with Laser Cooled Trapped Ions, *Phys. Rev. Lett.* **77**, 4728 (1996).

[65] Z. H. Yang, Y. P. Wang, Z. Y. Xue, W.-L. Yang, Y. Hu, J.-H. Gao, and Y. Wu, Circuit quantum electrodynamics simulator of flat band physics in a Lieb lattice, *Phys. Rev. A* **93**, 062319 (2016).

[66] D.-J. Zhang, Q.-H. Wang, and J. Gong, Quantum geometric tensor in PT -symmetric quantum mechanics, *Phys. Rev. A* **99**, 042104 (2019).

[67] L. Liang, T. I. Vanhala, S. Peotta, T. Siro, A. Harju, and P. Törmä, Band geometry, Berry curvature, and superfluid weight, *Phys. Rev. B* **95**, 024515 (2017).